Science Advances

AAAS

advances.sciencemag.org/cgi/content/full/2/3/e1501496/DC1

Supplementary Materials for

Designing durable icephobic surfaces

Kevin Golovin, Sai P. R. Kobaku, Duck Hyun Lee, Edward T. DiLoreto, Joseph M. Mabry, Anish Tuteja

Published 11 March 2016, *Sci. Adv.* **2**, e1501496 (2016)
DOI: 10.1126/sciadv.1501496

This PDF file includes:

Other Supplementary Material for this manuscript includes the following:
(available at advances.sciencemag.org/cgi/content/full/2/3/e1501496/DC1)

Icephobicity of Metal Meshes

Metal meshes were coated with PDMS + silicone oil mixtures to elucidate the effects of porosity on τ_{ice}, in spite of condensation. Each mesh, when tested, was suspended on glass slides ~1mm thick with the area directly below the column of water open to air (inset, Fig. S5g). In this way, condensation occurred on the Peltier plate beneath the mesh, but did not reach the column of water during testing. At a Peltier plate temperature of -10°C, for a suspension height of 1mm, we found the mesh surface temperature to be around -8°C. Other experiments indicate that there is a negligible difference in τ_{ice} measured at -8°C and -10°C. Wetted fractions, % open area and surface roughness could all be considered constant for any given mesh. To find the exact surface area in contact with water during testing, we first derive the surface area of a single metal wire with diameter *D*.

Water comes in contact with the top of each wire until locally the Young's relation has been achieved, i.e. the angle made at the three-phase contact line is the equilibrium contact angle θ_y.

From geometry, $\frac{\pi}{2} = (\pi - \theta_y) + (\frac{\pi}{2} - \alpha)$, where α is defined in the inset of Fig. S5e.

From this we find $\frac{\alpha}{2\pi} = \frac{SA_{wire}}{2\pi D}$ as we have only considered one half of the wire. Finally,

$$SA_{wire} = D(\pi - \theta_y). \quad (2)$$

For a given mesh, the mesh number *M* is defined linearly as the number of cells per inch. Thus there are 2*M* wires in any in^2. We must be careful to not double count the surface area from the overlap of wires within the weave. There are M^2 total of these overlaps. We then write,

$$SA_{mesh} = 2M * D(\pi - \theta_y) - DM^2 * D(\pi - \theta_y) \quad (3)$$

$$SA_{mesh} = DM(\pi - \theta_y)(2 - DM) \quad (4)$$

If we consider a unit cell of a mesh, the area contains one cell of the mesh, along with two wires, with an overlapping area of D^2. The side length of this unit cell is simply 1/*M*, whereas the side length of the open area is 1/*M* – *D*. The open area *OA* is then,

$$OA = \frac{(1/M - D)^2}{(1/M)^2} \quad (5)$$

Which simplifies to

$$OA = 1 - DM(2 - DM) \quad (6)$$

The total parameter space of metal meshes studied can be seen in Fig. S5a. When coating the meshes we used solutions with a polymer concentration of 200 mg/ml in hexane. Coating thickness could alter the above calculations, and thus we experimented to find a coating thickness that minimally altered the dimensions of the mesh while still providing complete surface coverage (Fig. S5b,c). The optical image of the test setup shown in Fig. S5d highlights

how frosting is a major concern for textured surfaces in the Cassie-Baxter state. Underneath the freezing column of water frost is prominently visible, but it did not affect our measurements.

We tested four meshes of differing diameter but constant 30% *OA* (Fig. S5f) and five meshes with constant diameter (140μm) and differing *OA* (Fig. S5e). We found a linear relationship with τ_{ice} between both *OA* and D^2. Moreover, we found that D^2r correlated best with τ_{ice} for all the meshes we tested (Fig. S5g). Here *r* is the Wenzel roughness, which is the nondimensional form of SA_{mesh} (which is defined per in^2).

I^* derivation

To find I^* we take two surfaces with the same ρ^{CL}. The first does not have interfacial slippage and has an ice adhesion strength denoted $\tau_{ice}^{no-slip}$. Similarly, the second surface has interfacial slippage and is denoted τ_{ice}^{slip}. We subtract the second surface from the first,

$$\ln(\tau_{ice}^{no-slip}) - \ln(\tau_{ice}^{slip}) = \frac{1}{2}\ln(\rho^{CL}) - \ln(\rho^{CL}) + C \tag{7}$$

I^* easily follows by simplifying the natural logarithms.

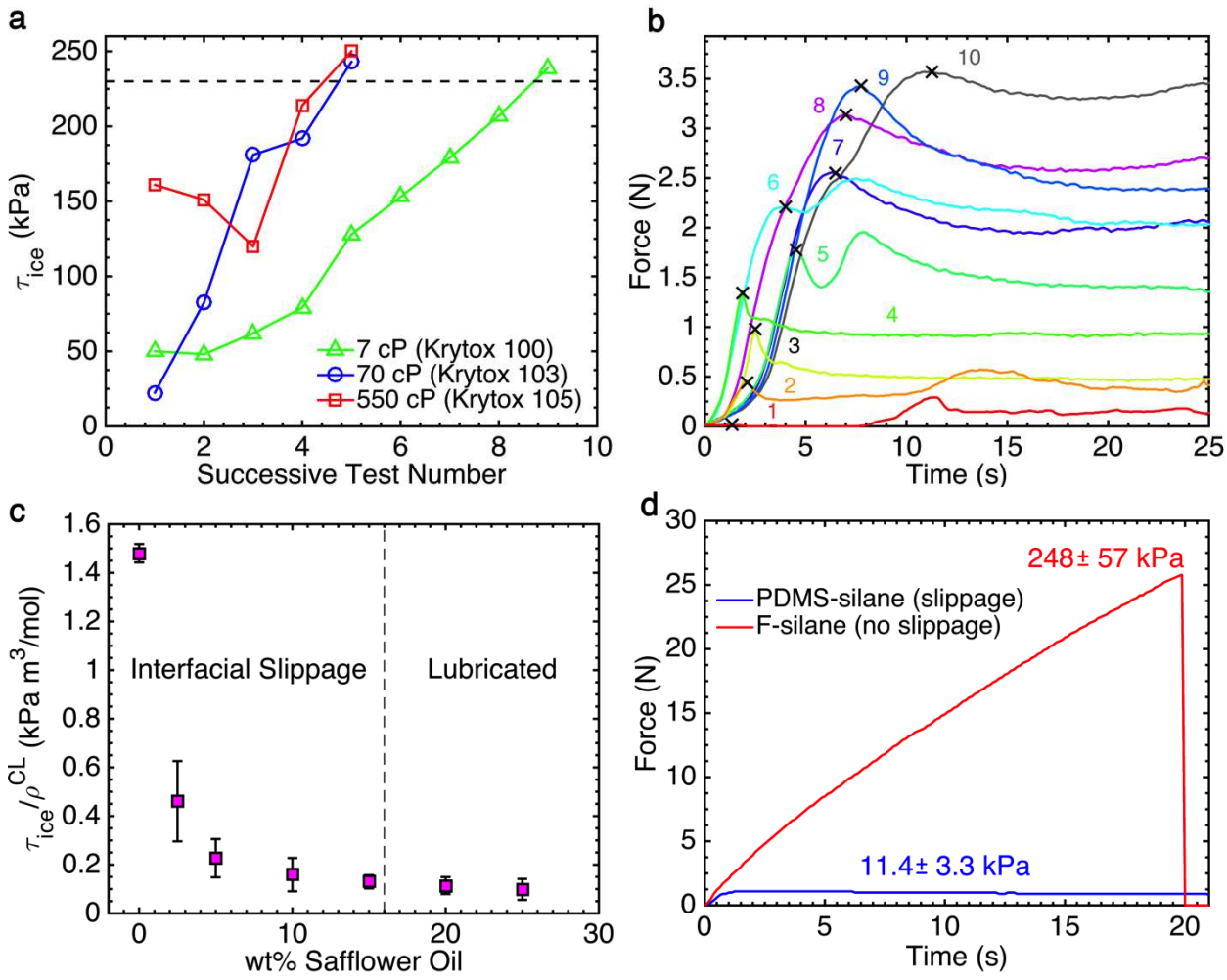

Fig. S1. Liquid layer surface degradation. a, Variation of τ_{ice} with the number of icing / deicing cycles for SLIPS-based (*27*) icephobic surfaces. **b,** The force vs. time curves for coating **Q**, comprised of Sylgard 184 PDMS with a 1:1 base:crosslinker ratio and 75wt% silicone oil (Table S1), which has an initial ice adhesion strength of 0.15 kPa. The 'x' symbol denotes the time when ice first un-adhered from the coating. **c,** The effect of oil content in our PU on τ_{ice} after normalizing by ρ^{CL}. The miscibility limit of safflower oil is ~ 16wt%. It is clear that once the oil starts to phase separate from the PU elastomer, the mechanism for reduced ice adhesion transitions from interfacial slippage to lubrication. **d,** When treated with a PDMS-silane, surfaces exhibit interfacial slippage and consequently low ice adhesion. Fluoro-silanes, known to not exhibit interfacial slippage (*27*), show relatively high ice adhesion, in spite of their low solid surface energy.

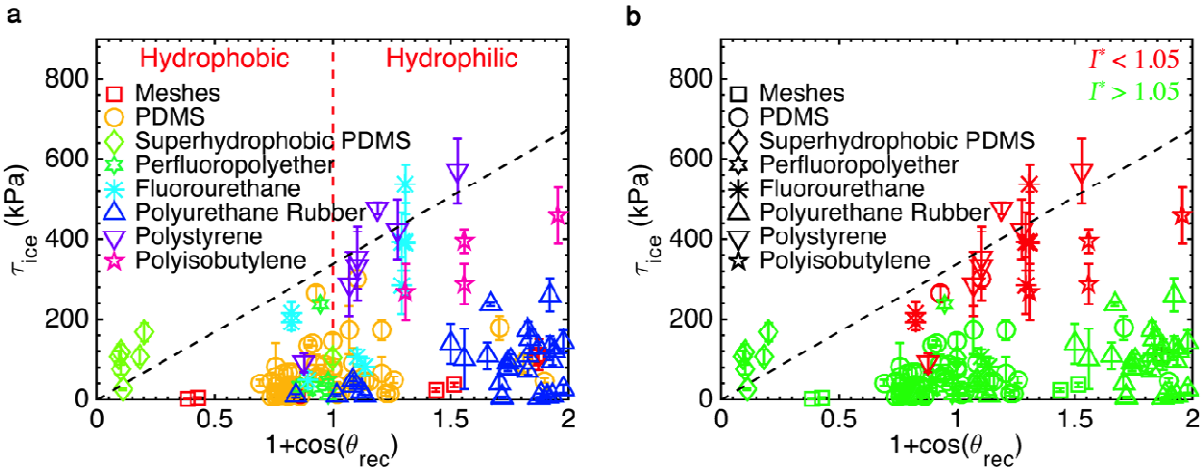

Fig. S2. **Surface chemistry independence. a,** The various icephobic surfaces fabricated in this work. It is clear that most of the fabricated surfaces do not follow the theoretical $\tau_{ice} \propto 1+\cos\theta_{rec}$ trend. For example, for coating AY (Table 1), τ_{ice} = 27±10 kPa, although θ_{rec} = 12°. **b,** When recolored using the developed I^* parameter (with a cutoff of I^* = 1.05), it is apparent that the linear trend between ice adhesion and surface energy only applies for high modulus (I^* < 1.05) elastomers without interfacial slippage.

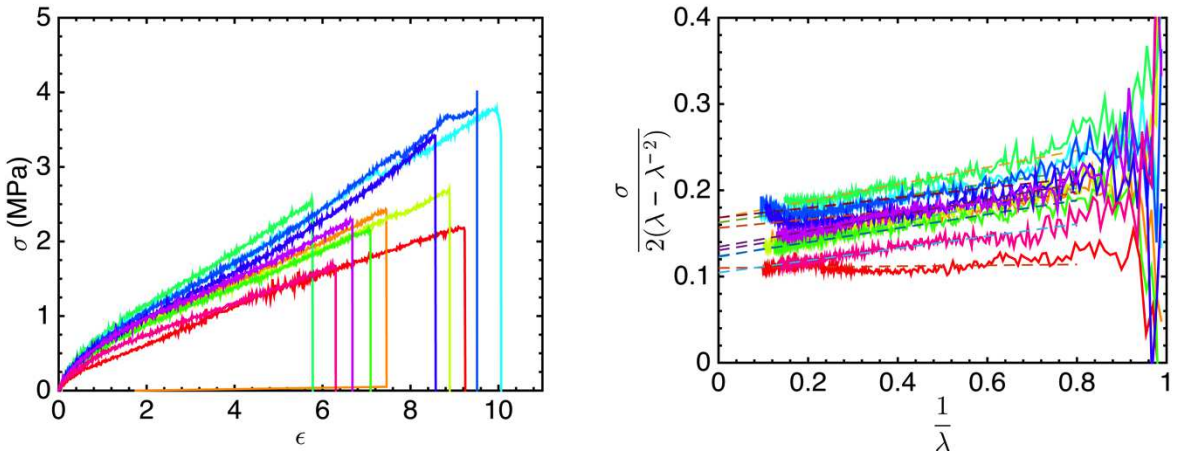

Fig. S3. Tensile test data. a, Stress-strain results for our icephobic polyurethane rubber (Vytaflex 40, 15 wt% safflower oil). Note the elongations at break are in excess of 1000%. b, Re-plotting the data using Mooney-Rivlin axes allows ρ^{CL} to be computed (intercept of the y-axis at infinite elongation). Due to inaccuracies of the test machine at very small strains, linear regressions for the stress-strain data were fit when $1/\lambda \leq 0.8$, where λ is the extension ratio. For all the materials tested, error between swelling studies and tensile test data was typically < 5%. The error between measured samples was usually much larger than the test method discrepancy, i.e. the two test methods gave statistically equivalent crosslink densities, with an overall uncertainty of around 10%.

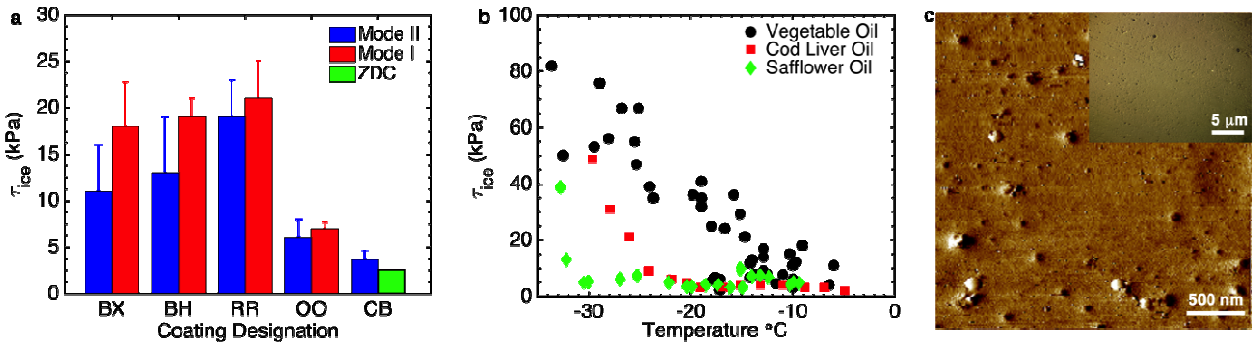

Fig. S4. Interfacial slippage mechanism additional data. a, Comparison of five samples (BX: PU+15 wt% vegetable oil, BH: PDMS-modified PU+10 wt% silicone oil, RR: low ρ^{CL} PDMS without oil, OO: low ρ^{CL} PDMS + 25 wt% silicone oil, CB: PU+15 wt% safflower oil, see Table S1) sent to CRREL compared to data taken in-house. Note that CRREL data points (Mode-I) are the average of two different samples tested once, whereas the in-house data points (Mode-II) are the average of at least 10 subsequent measurements. Mode-I is defined by tensile loading at the ice-substrate interface, whereas Mode-II is defined by shear loading at the ice-substrate interface (*27*). The zero-degree-cone test (ZDC) is an alternate method of evaluating Mode-II ice adhesion. **b,** Low temperature studies for the polyurethane filled with 15wt% vegetable, cod liver or safflower oil. The increase in ice adhesion indicates the loss of interfacial slippage, caused by the freezing of the fatty acid chains. The polyunsaturated fatty acid content increases from vegetable to cod liver to safflower oil. **c.** AFM phase image of the PU coating without oil.

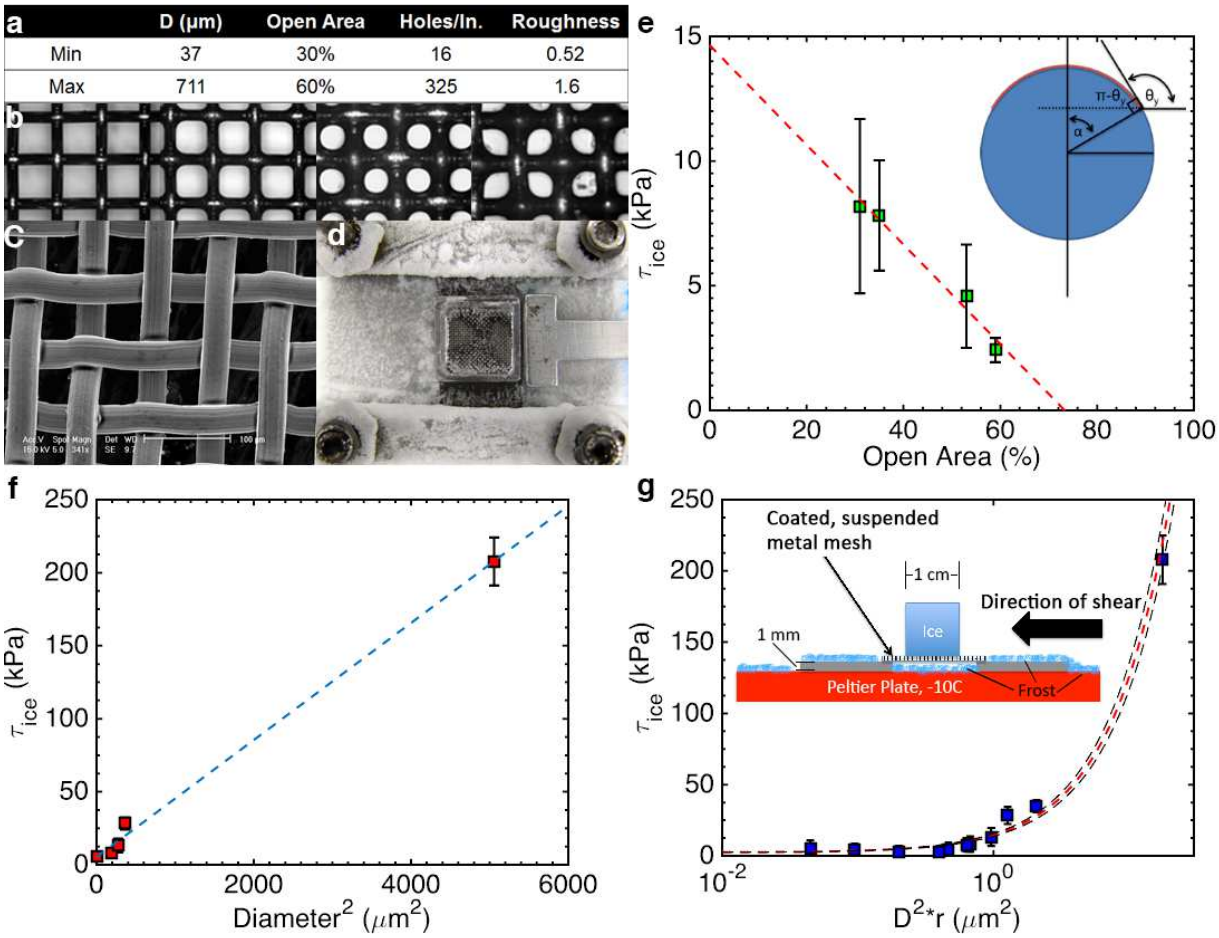

Fig. S5. Icephobicity of coated meshes. a, The parameter space of mesh properties evaluated. **b,** The effect of dip coat solution concentration on % open area. **c,** SEM micrograph of a PDMS coated, mesh 500. **d,** Frost all around our ice testing setup, including underneath the suspended mesh. **e,** τ_{ice} versus the % open area of meshes with D = 140 μm. **f,** τ_{ice} versus D^2 for meshes with an open area of 30%. **g,** τ_{ice} for a coated mesh correlates very well with the predictor D^2r, where r is the Wenzel roughness and D is the wire diameter. The low interfacial area between ice and the substrate can significantly lower τ_{ice}. A PDMS-coated (ρ^{CL} = 219±13 mol/m^3, 25wt% 100cP silicone oil) mesh with a wire diameter of 140μm and an open area of 59% displayed τ_{ice}^{mesh} = 2.4±0.5 kPa, whereas τ_{ice}^{smooth} = 35±5 kPa. The inset shows the experimental setup for suspended metal mesh ice adhesion testing.

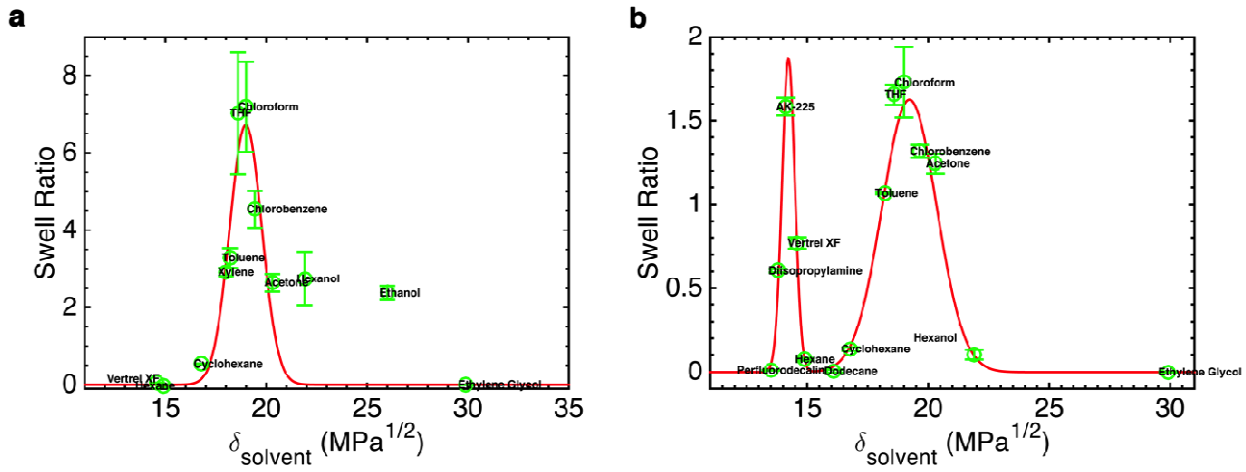

Fig. S6. Elastomer solubility parameter determination. a, Equilibrium swell ratios for the PU as a function of the probe solvent's solubility parameter, $\delta_{solvent}$. The data is fitted to a Gaussian. **b,** Equilibrium swell ratios for the FPU as a function of $\delta_{solvent}$. The data is fitted to a bi-modal Gaussian, accounting for the swelling of the fluorinated and urethane components independently. The peak around 19 $MPa^{1/2}$ is characteristic or the urethane bond (*27*).

Movie S1 Caption

A droplet of water dyed green is frozen on one of our most icephobic surface (coating Q in Table S1) at -18°C. This specimen was spray-coated with a 500mg/ml polymer solution in hexane (10mL total). Once the water turns to ice, the surface is slanted, and the ice slides off under its own weight.

Movie S2 Caption

This movie shows an icephobic polyurethane sample ($\tau_{ice} \approx 20$ kPa) that we have molded into a slab. One end of the slab is clamped in a vice, the other is free to pull. When subjected to a strain of ~350%, the elastomer is still in tact with no signs of tearing or breakage. Upon removal of the load, the rubber returns to its original length, pointing towards fully elastic deformation. When such a surface is subsequently tested for ice adhesion, the τ_{ice} is unchanged before and after mechanical deformation.